Pharm Res (2014) 31:3161–3178
DOI 10.1007/s11095-014-1409-0

RESEARCH PAPER

Concentration Dependent Viscosity of Monoclonal Antibody Solutions: Explaining Experimental Behavior in Terms of Molecular Properties

Li Li • Sandeep Kumar • Patrick M. Buck • Christopher Burns • Janelle Lavoie • Satish K. Singh • Nicholas W. Warne • Pilarin Nichols • Nicholas Luksha • Davin Boardman

Received: 19 December 2013 / Accepted: 6 May 2014 / Published online: 7 June 2014

ABSTRACT

Purpose Early identification of monoclonal antibody candidates whose development, as high concentration (≥100 mg/mL) drug products, could prove challenging, due to high viscosity, can help define strategies for candidate engineering and selection.

Methods Concentration dependent viscosities of 11 proprietary mAbs were measured. Sequence and structural features of the variable (Fv) regions were analyzed to understand viscosity behavior of the mAbs. Coarse-grained molecular simulations of two problematic mAbs were compared with that of a well behaved mAb.

Results Net charge, ξ-potential and pI of Fv regions were found to correlate with viscosities of highly concentrated antibody solutions. Negative net charges on the Fv regions of two mAbs with poor viscosity behaviors facilitate attractive self-associations, causing them to diffuse slower than a well-behaved mAb with positive net charge on its Fv region. An empirically derived equation that connects aggregation propensity and pI of the Fv region with high concentration viscosity of the whole mAb was developed.

Conclusions An Fv region-based qualitative screening profile was devised to flag mAb candidates whose development, as high concentration drug products, could prove challenging. This screen can facilitate developability risk assessment and mitigation strategies for antibody based therapeutics *via* rapid high throughput material-free screening.

L. Li • C. Burns • J. Lavoie • N. W. Warne • P. Nichols • N. Luksha • D. Boardman
Biotherapeutics Pharmaceutical Sciences Research and Development
Pfizer Inc., 1 Burtt Road, Andover, Massachusetts, USA

S. Kumar (✉) • P. M. Buck • S. K. Singh
Biotherapeutics Pharmaceutical Sciences Research and Development
Pfizer Inc., 700 Chesterfield Parkway West, Chesterfield
Missouri 63017, USA
e-mail: Sandeep.Kumar@pfizer.com

KEY WORDS concentration · electrostatics · formulation · molecular modeling · monoclonal antibodies · subcutaneous delivery · viscosity

ABBREVIATIONS

$<x^2>$	Average mean squared displacement
CDR	Complementarity determining region
C_H1	First domain in constant portion of a heavy chain
C_H2	Second domain in constant portion of a heavy chain
C_H3	Third domain in constant portion of a heavy chain
cIEF	Capillary Iso-Electric Focusing
cP	Centi Poise
D	Diffusion coefficient
D_{Fv}	Dipole moment for Fv portion of a mAb
$D_{whole\ mAb}$	Dipole moment of a full length mAb
Fab	Fragment antigen binding
Fc	Fragment crystallize-able
Fv	Fragment variable
GB/VI	Generalized Born/Volume Integral
IgG	Immunoglobulin G
k_B	Boltzmann constant
KD hydromom$_{Fv}$	Kyte-Doolittle hydrophobicity moment for Fv portion of a mAb
LAMMPS	Large-scale Atomic/Molecular Massively Parallel Simulator
mAb	Monoclonal antibody
MOE	Molecular Operations Environment
NormASAhphob	Normalized hydrophobic surface area
$Nres_{Fv}$	Number of residues in the Fv region
$PaggTANGO_{Fv}$	Normalized aggregation propensity of an Fv region computed by using TANGO
$P_{agg}Waltz_{Fv}$	Normalized aggregation propensity of an Fv region computed by using Waltz
pI_{Fv}	Isoelectric point for Fv portion of a mAb

$pI_{whole\ mAb}$	Isoelectric point of a full length mAb
RMSE	Root Mean Square Error
RMSG	Root Mean Square Gradient
rpm	Revolutions per minute
UF/DF	Ultra-Filtration/Dia-Filtration
UV–vis	Ultraviolet–visible
V_H	Variable domain of a heavy chain
V_L	Variable domain of a light chain
$Z_{app\ whole\ mAb}$	Apparent charge on a full length mAb
Z_{appFv}	Apparent charge on Fv portion
$Z_{constant\ regions}$	Net charge on the constant regions of a mAb
Z_{Fv}	Net charge on Fv portion of a mAb
$Z_{whole\ mAb}$	Net charge on a full length mAb
η	Measured viscosity of an antibody solution
η_{rel}	Relative viscosity of an antibody
η_{sp}	Specific viscosity of an antibody
μ	Particle mobility
$\xi_{constant\ regions}$	Zeta potential of constant regions of a mAb
ξ_{Fv}	Zeta potential of Fv portion of a mAb
ξ-potential	Zeta potential
$\xi_{whole\ mAb}$	Zeta potential of a full length mAb

INTRODUCTION

Biopharmaceuticals, especially monoclonal antibodies (mAbs), have become one of the most therapeutically relevant classes of medicines in recent years. Most of the early mAb based therapeutic products required parenteral intravenous administration [1]. However, the ability to subcutaneously deliver small volumes (typically ~1 mL) of highly concentrated (often 100–150 mg/mL) antibody solutions is desirable from the perspective of patient convenience and compliance, particularly for chronic and/or home use [1, 2]. High concentration mAb products are therefore increasingly being developed in a variety of indications [1–3]. A potential issue faced during the development of such products is high viscosity which can result in challenges during manufacturing, processing and administration [4, 5]. Protein solutions with viscosities above ~20 cP at the target dose concentration can be difficult to inject (based on a 1 mL injection over 10 s from a standard 1-mL long syringe with a 27G 13 mm needle resulting in the relatively high glide force of ~28 N estimated using the Hagen-Poiseuille equation). Downstream ultra-filtration/dia-filtration (UF/DF) and concentration steps also become onerous [6]. A number of different approaches have been suggested to lower the viscosity of mAb solutions at high concentrations. These include the use of common salts [7], hydrophobic salts [8], polar solvents [9], non-aqueous organic suspensions [10] and gel beads [2]. Processing at higher temperatures (e.g. 35–40°C) has also been used to get around the viscosity issue [6]. However, practical avenues for addressing viscosity, once a molecule has been selected for development, are limited and resource-intensive.

A resource-sparing and more pragmatic approach would be to identify and eliminate molecules with high viscosity liability early in discovery, when multiple candidates are being examined from several perspectives. However, to enable this, high-throughput screening tools with little or no material needs, are required. Experimental approaches for high-throughput screening have been developed [11–13]. Computational methods of molecular modeling and data analyses would be uniquely suited for such applications, since these can be applied prior to starting any experimental work and/or when the material available for experimental studies is scarce. A major advantage with computational methods is that they can be easily programmed to work in high-throughput manner. Such methods can also be easily modified and improved with increased knowledge and experience. When applied in early stages of discovery, a degree of false-positives can also be tolerated since there are generally a large number of potential candidates to select from. The same tools can be used to strategically identify minor modifications to the amino acid sequences of lead candidate mAbs, that may result in lower viscosity at high concentrations (as well as potentially mitigate aggregation and improve solubility) without impacting their potency [14–22]. For example, Shire and coworkers have probed the influence of charged residues present in the CDRs on the viscosity behaviors of two mAbs using both experimental and computational methods. One mAb exhibited high viscosity at higher concentrations while the other one was well-behaved. Mutations in the CDRs of the first mAb shrank a large negatively charged patch and improved its viscosity behavior [22, 23].

Biophysical characteristics of concentrated antibody solutions are being studied *via* both experimental and computational means to understand the reasons behind high viscosity [7, 11, 24–29]. In highly concentrated antibody solutions, the individual antibody molecules are crowded together and distances between them can be of the same order of magnitude as the size of the molecules [30]. In these crowded molecular environments, close-range inter-molecular interactions, both electrostatic and hydrophobic, become highly significant which can lead to non-ideal solution behavior [30]. Surface electrostatic properties of the antibody molecules are also thought to play important roles in determining their concentration dependent viscosity behaviors [23, 29, 31, 32]. Two-dimensional correlation vibrational spectroscopic experiments using FTIR and principal component analyses performed by Kamerzell and coworkers on two IgG1κ mAbs with identical framework regions but different CDRs, indicate that conformational heterogeneity and hydrogen bonding networks modulate self-association behavior of the two mAbs from low to high concentrations [25]. Similarly, measurements of the interaction parameter (k_D) *via* dynamic light scattering (DLS) or second virial coefficient *via* analytical ultracentrifugation (AUC) experiments performed at low concentrations may indicate whether

highly concentrated solutions of a mAb will exhibit undesirable rheological characteristics [12, 29, 33].

The goal of the present work was to identify molecular properties, calculated using commonly available software, which may relate to the viscosity behavior of highly concentrated antibody solutions. Such properties can help construct qualitative molecular screening profiles useful for 'red flagging' problematic candidates at early stages of drug discovery. In this work, we have obtained concentration dependent viscosity data for 11 therapeutic mAbs using identical experimental procedures, instruments and formulation buffer that contained no added salt to facilitate direct comparisons among the mAbs. Several sequence and structure based electrostatic and hydrophobic descriptors were computed for the Fv regions of these 11 mAbs using identical computational modeling procedures and software. Statistical analyses were performed to identify potential descriptors that correlate with viscosities of highly concentrated antibody solutions. All the results were interpreted in terms of general electrostatic properties of human mAbs.

Most constant domains in human antibodies have pI values ≥6.5. Therefore, these domains have positive net charges (+ve $Z_{\text{constant regions}}$) and positive ξ-potentials (+ve $\xi_{\text{constant regions}}$) in the optimum formulation pH range (5.5–6.3) for high concentration mAb formulations [34]. These observations imply that colloidal interactions involving only the constant regions of mAbs should be predominantly repulsive under the above conditions. Hence, electrostatic features of the variable regions (Fv) of mAbs play significant roles in determining their high concentration solution behaviors. Qualitative mAb candidate screening profiles based on calculated values of net charge, ξ-potential and pI of their variable regions (Z_{Fv}, ξ_{Fv} and pI_{Fv}) were devised here. These screens are capable of flagging problematic mAb candidates at early stages of biotherapeutic drug discovery. An empirical relationship which connects calculated structure-based pI and propensity for aggregation (calculated using amino acid sequences) of the Fv regions with viscosity of the full length mAbs at 150 mg/mL was also derived using regression analyses. In addition to these, an attempt was also made to understand the impact of inter-molecular interactions on mobility of the antibody molecules. Coarse-grained simulations were performed to investigate the diffusion behavior (indicative of self-associative property) of two problematic mAbs (mAbs 10 and 11) and a well-behaved mAb (mAb1). The problematic mAbs 10 and 11 were found to diffuse slower than the well-behaved mAb 1 at both low and high concentrations.

MATERIALS AND METHODS

Materials

All 11 proprietary mAbs were manufactured at Pfizer (Andover, MA). All mAbs were produced in CHO cells followed by a two or three column purification train designed to meet GMP specifications of high quality and purity, with low aggregate levels (<5%). Therefore, all materials are of GMP grade and were subjected to release testing for clinical use. Glycan analyses suggested similar glycan profiles for all mAbs in this study. There are four IgG1λ, three IgG1κ, two IgG2κ and two IgG4κ mAbs in this study.

Viscosity Measurements

All viscosity measurements were carried out in the same formulation buffer composition and experimental conditions. Viscosity data were generated on 11 mAbs prepared in the following formulation buffer: 20 mM histidine/histidine-HCl buffer, 50 mg/mL sucrose, 0.05 mg/mL $Na_2EDTA.2H_2O$ and 0.2 mg/mL polysorbate 80 (PS-80) at pH 5.8. All samples were dialyzed extensively against their off-set buffers containing neither sucrose nor PS-80. The off-set buffers were designed based on a method developed by Bolton *et al.* [35]. This method was demonstrated to be sufficient for overcoming the Donnan effect at high concentrations. Note that there is no added salt in the formulation buffer and all the samples were dialyzed extensively so that ions carried over from the purification train are removed as much as possible. All mAbs were concentrated to their solubility limits in the off-set buffers using Pall 10 kDa Advanced Macrosep centrifugal concentrators. Sucrose and PS-80 were then spiked to these concentrates to the target level of 50 mg/mL and 0.2 mg/mL, respectively. All samples were filtered through 0.22 μm syringe filters, and then diluted to different target concentrations (such as 150 mg/mL, 100 mg/mL and so on) in the formulation buffer.

Protein concentrations were determined by A280 analysis utilizing a UV–vis spectrophotometer equipped with a SoloVPE variable path-length attachment. Viscosity measurements on all 11 mAbs were performed using an Anton Paar CP25-1 cone & plate rheometer at a rotational speed of 150 rpm at 25°C (shear rate, 900 s^{-1}). All sample aliquots were analyzed at this fixed shear rate for 10 measurements over duration of 100 s. No significant change in the viscosity values was observed among different measurements, indicating that the solutions are Newtonian. The viscosity measurements were performed with two fresh aliquots of the samples, and the average and standard deviations values for the solution viscosity (η) were computed using all twenty readings. These data are reported in Table I. Viscosity data at 150 mg/mL mAb concentration were used for the purpose of assessing correlations between high concentration viscosity and different molecular properties of the mAbs computed *via* molecular models and amino acid sequences of their Fv portions.

Table I Concentration Dependent Viscosity Data on 11 mAbs Used in this Study*

mAb #, Isotype, pI‡	C_{20}	η (cP)	C_{50}	η (cP)	C_{75}	η (cP)	C_{100}	η (cP)	C_{125}	η (cP)	C_{150}	η (cP)	C_{175}	η (cP)	C_{200}	η (cP)
1, IgG1κ, 8.3	19	1.1 ± 0.0	49	1.5 ± 0.0			98	2.6 ± 0.0	126	3.7 ± 0.0	153	5.4 ± 0.1	172	8.0 ± 0.1	204	13.5 ± 0.2
2, IgG1κ, 8.7	18	1.2 ± 0.0	52	1.6 ± 0.0			97	2.7 ± 0.0	127	3.7 ± 0.1	149	5.4 ± 0.1	171	8.1 ± 0.2	195	13.3 ± 0.7
3, IgG4κ, 7.5	23	1.2 ± 0.0	46	1.5 ± 0.0			95	2.9 ± 0.1	126	4.0 ± 0.0	148	6.2 ± 0.1	171	11.1 ± 0.6	198	19.1 ± 3.7
4, IgG1λ, 8.7	19	1.1 ± 0.0	45	1.4 ± 0.0			99	2.7 ± 0.0	126	4.1 ± 0.1	147	6.6 ± 0.1	176	12.2 ± 0.6	196	20.4 ± 0.9
5, IgG1κ, 8.1	21	1.2 ± 0.0	48	1.7 ± 0.0	74	2.3 ± 0.0	98	3.3 ± 0.0	129	5.3 ± 0.0	150	8.4 ± 0.1	175	14.1 ± 0.2	203	28.9 ± 0.8
6, IgG1λ, 8.2	25	1.3 ± 0.0	49	1.7 ± 0.0			105	3.9 ± 0.0	127	6.9 ± 0.0	153	12.9 ± 0.1	183	27.6 ± 0.2		
7, IgG2κ, 6.9	19	1.1 ± 0.0	53	1.5 ± 0.0			96	3.2 ± 0.2	125	6.4 ± 0.6	150	13.9 ± 0.5	170	27.3 ± 4.5		
8, IgG4κ, 7.0	17	1.2 ± 0.0	43	1.5 ± 0.0	91	3.3 ± 0.0	114	5.0 ± 0.1	137	8.3 ± 0.1	160	14.5 ± 1.1			189	33.0 ± 2.7
9, IgG2κ, 7.4	25	1.3 ± 0.0	50	1.7 ± 0.0			107	4.2 ± 0.1	134	7.6 ± 0.1	155	15.6 ± 0.6			191	44.9 ± 1.8
10, IgG1λ, 7.2	19	1.2 ± 0.0	52	2.5 ± 0.0			103	15.4 ± 0.2	131	43.6 ± 0.6	149	94.7 ± 0.6				
11, IgG1λ, 6.9	20	1.6 ± 0.0	41	3.4 ± 0.0	81	15.4 ± 0.1	106	30.2 ± 0.2	130	57.9 ± 0.5	150	103.6 ± 1.0				

*Measured concentration dependent solution viscosity data for 11 mAbs. Viscosities were measured at several targeted concentrations. For example, C_{20} means experimentally measured concentration at targeted concentration value of 20 mg/mL. The values shown in this table are for solution viscosity (η). These data were used to derive values for specific viscosity (η_{sp}) and relative viscosity (η_{rel}) of the mAbs plotted in Fig. 1. ‡pI values reported in this table were measured using cIEF method described in the text. The highly concentrated solutions of mAbs 10 and 11 show high viscosities.

Mathematical Manipulation of Viscosity Data

Experimentally measured viscosity data on antibody solutions was manipulated according to viscosity and concentration relationships described in chapter 15 of the book "The physical and chemical basis of molecular biology" by Creighton [36] and in the report by Lileystrom *et al.* [7]. In particular, the following equations were used:

$$\eta = \eta_o\left(1 + k_1 c + k_2 c^2 + k_3 c^3 + \ldots.\right) \quad (1)$$

$$\eta_{rel} = \eta/\eta_o \quad (2)$$

$$\eta_{sp} = \eta_{rel} - 1 \quad (3)$$

Where, c, η, η_{rel} and η_{sp} are concentration, solution viscosity, relative viscosity and specific viscosity of a mAb, respectively. Viscosity of the solvent (formulation buffer), η_o, was measured to be 1.13 cP (25°C). k_1, k_2, k_3 … are constants. The concentration dependent viscosity curves of the 11 mAbs were obtained by plotting η_{sp}/c *versus* c.

Determination of pI by Capillary Iso-Electric Focusing (cIEF)

The cIEF analyses were performed using a Beckman Coulter PA800 Capillary Electrophoresis System and the Advanced cIEF Starter Kit (Beckman Coulter, Inc., Fullerton, CA). Anolyte, catholyte, anodic stabilizer, cathodic stabilizer, chemical mobilizer, urea, and urea/gel solutions were prepared according to the manufacturer instructions included in the reagents kit. The capillary was a Neutral capillary (50 μm I.D. × 45 cm) from Beckman Coulter. UV detection was carried out with a 280 nm filter. Electropherograms were analyzed using Waters Empower™ software. The pI marker samples were run immediately before each protein sample. The experimental pI values were determined by creating a standard curve from the pI markers and comparing the migration time of the protein peak to the curve.

Structural Model Building of Fv Regions of 11 mAbs

Molecular models for Fv regions of 11 mAbs were made using the Antibody Modeler module in MOE2012.10. For each mAb, up to 625 intermediate homology based models (25 backbone models and 25 side chain models per backbone model) were made for the Fv region. The intermediate models were optimized to Root Mean Square Gradient (RMSG) of 0.01 *via* energy minimizations using AMBER99 Force-field with Reaction field implicit solvation model. The internal dielectric was set to 4 and external dielectric was 80. Cut off distances of 10 and 12 Å were used to screen non-bonded interactions. The

intermediates were ranked according to their GB/VI scores and the model with the highest rank was selected as the final model for the Fv portion of each mAb. The C-termini of V_L and V_H domain in the final model were neutralized *via* amidation and the model was re-protonated to mimic pH 5.8 and zero salt concentration *via* Protonate3D in the Structure Preparation module of MOE2012.10. After these steps were complete, the final model was optimized *via* energy minimizations to RMSG below 0.00001.

Computation of Molecular Properties

The final energy minimized models of the Fv portions of the 11 mAbs were used to compute molecular properties at pH 5.8 and 1 mM NaCl concentration (low ionic strength) using the Protein Properties module in MOE2012.10. Hydrophilic (positively and negatively charged) and hydrophobic surface patches were also computed using the default options in MOE2012.10. The following set of protein properties were computed using the Fv models: Net Charge (Z_{Fv}), Apparent charge (Z_{appFv}), Dipole moment (D_{Fv}), Kyte-Doolittle hydrophobicity moment (KD hydromom$_{Fv}$), ξ-Potential (ξ_{Fv}), pI (pI_{Fv}), hydrophobic and hydrophilic Van der Waals surface area, electrophoretic mobility, hydrodynamic radius, radius of gyration, and number of large (greater than 100 Å^2) positively charged, negatively charged and hydrophobic surface patches. The net charge (Z_{Fv}) *versus* pH titration curves were computed for the Fv regions of all mAbs in the pH range 3 to 13 using protein properties module in MOE2012.10.

Protein properties and titration curves were also computed for the constant domains of a human IgG1κ mAb using the atomic coordinates for these domains obtained from the crystal structure of human b12 antibody [37] available from the Protein Data Bank [38] (PDB, http://www.rcsb.org/pdb/home/home.do) entry 1HZH. Furthermore, similar calculations were also performed for other constant domains types, namely, C_L domain of a human λ light chain, human IgG2 Fc dimer and components, and human IgG4 Fc dimer and components using crystal structure data contained in the PDB entries 2MCG, 4HAG and 4C54 respectively.

Sequences of the Fv portions of these mAbs were also used for calculation of aggregation propensity [17] and hydrophobicity. The aggregation propensities were calculated using TANGO [39] and WALTZ [40]. The hydrophobicities were computed using an in-house developed program that is based on a scale proposed by Hodges and coworkers [41]. For each Fv region, normalized values of the sequence based properties (TANGO/WALTZ aggregation propensities and hydrophobicity) were computed as follows:

$$P_{Norm} = \frac{(TotP_{LC} + TotP_{HC})}{Nres_{Fv}} \quad (4)$$

Where, P_{Norm} is the normalized value of the TANGO aggregation score, WALTZ aggregation score or hydrophobicity. $TotP_{LC}$ and $TotP_{HC}$ are the total values of TANGO aggregation score, WALTZ aggregation score or hydrophobicity for all heavy and light chain residues within the Fv. $NRes_{Fv}$ is the total number of residues in the Fv. Normalized values of the hydrophobic surface area were also calculated in an analogous way. In total, 18 different descriptors computed from sequence and structural models of the Fv regions, were analyzed for their correlation with concentration dependent viscosity behaviors of the full length mAbs.

Curve Fitting and Data Analyses

The results of concentration dependent viscosity measurements of 11 mAbs were analyzed for the relationship between viscosity and mAb concentration *via* curve fitting tools available in MATLAB R2013a from MathWorks, Inc. These tools were also used to explore correlation between molecular properties computed from sequence and structural models of the Fv portions and experimentally obtained viscosity data of the 11 full length mAbs.

Coarse-Grained Simulations

The full length structure of the human IgG1 b12 antibody, PDB entry 1HZH, was used to create a twelve bead coarse-grained antibody representation. A single interaction bead was placed at the center of mass of each antibody structural domain (V_L, C_H1, C_H3 *etc.*). The mass of each bead was determined by summing all atomic masses assigned to the coarse-grained (CG) interaction site. CG interactions sites, representing constant regions, were assigned point charges based on the average net charges for the constant domains of the b12 antibody (Table III). CG interaction sites representing the variable region were assigned point charges based on the net charge for Fv regions calculated for each of the mAbs used in this study (Table V). This yielded distinct electrostatic features for individual coarse-grained mAbs. For three of these mAbs (mAb1, mAb10, and mAb11), multi-copy (512 copies) mAb simulations were run to estimate the diffusion coefficients at concentrations of 30 mg/mL and 100 mg/mL. Each simulation was performed using LAMMPS [42] (http://lammps.sandia.gov/index.html) and run *in vacuo* with periodic boundary conditions at 300 K for 5 μs with a time step of 1 ps. Electrostatic interactions were modeled with a Coulombic potential and a Yukawa term to capture the effect of screening.

$$U_{Coul} = \frac{q_i q_j}{4\pi\varepsilon}\exp(-\kappa r) \quad (5)$$

Where, q_i and q_j represent the net charges on interaction beads, and ε represents the effective dielectric constant. The Debye screening length (inverse of screening parameter κ) was

set to 25 Å. In this study, we assumed a screened implicit solvent model with an effective dielectric constant of 1. A Lennard-Jones 12–6 potential was used to model repulsive and attractive interactions. Further details on the set-up of the coarse-grained simulations performed in this study can also be found elsewhere [27, 28]. During simulations, coarse-gained mAbs were treated as rigid molecules to prevent intramolecular fluctuations.

To estimate the impact of intermolecular interactions between mAb molecules, the translational diffusivity (or Diffusion coefficient, D) was computed [36]. According to the Einstein-Smoluchowski relation ($D=\mu\ k_BT$), diffusivity D is proportional to particle mobility μ. Furthermore, it can be shown that the mobility for a spherical particle is inversely related to its radius *r* and solution viscosity η yielding $\mu=(6\eta\pi r)^{-1}$. Combining the two previous equations yields the Stokes-Einstein equation $D=k_BT\ (6\eta\pi r)^{-1}$, which establishes a relationship between particle diffusion and solution viscosity through the spherical radius of the particle [36]. Thus by calculating the diffusion coefficient, one can estimate solution viscosity; however, lacking the Stokes particle radius r, our results from coarse-grained simulations only provide estimates of diffusion coefficient. In homogenous solutions, the diffusion coefficient can be calculated using the Einstein relationship for Brownian motion, which relates the mean squared displacement for particles to diffusion and time *t*, $<x^2> = 6Dt$ [36]. Here, diffusion coefficients of mAbs 1, 10 and 11 were estimated by plotting $<x^2>$ *versus t* in two five microseconds coarse grain simulations performed at different concentrations, namely 30 mg/mL and 100 mg/mL, for each mAb.

RESULTS

General Observations from Viscosity Behaviors of 11 mAbs

Table I compares the solution viscosity values for 11 mAbs at different target concentrations. These viscosity measurements were performed using the same instruments, experimental parameters and the same formulation buffer that contained no added salt. Therefore, it is feasible to directly compare concentration dependent viscosity behaviors of different mAbs in this dataset. The mAbs in Table I are numbered according to their increasing viscosity values at 150 mg/mL. At 20 mg/mL, all mAbs showed similar viscosity values, although the viscosity of mAb 11 is already greater than that of the other mAbs. As the concentrations increased, two mAbs, mAb 10 and mAb 11, began to show higher viscosity values than the other mAbs. By 150 mg/mL, the antibody solutions for these two mAbs were substantially more viscous than the other mAbs, with mAb 11 showing the highest viscosity (Table I).

The dataset of 11 mAbs used in this study comprises different isotypes that have been used to develop commercial biotherapeutic drug products by the pharmaceutical industry [16]. No correlation was observed between the isotypes and viscosity behaviors of the mAbs. Solutions of mAb 10 and mAb 11 were highly viscous at 150 mg/mL ($\eta=94.7\pm0.6$ cP for mAb 10, and 103.6 ± 1.0 cP for mAb 11). Both these mAbs are of the IgG1 λ isotype. Table I shows that mAb 4 and mAb 6, which are also IgG1 λ mAbs, had substantially lower viscosity values at 150 mg/mL ($\eta=6.6\pm0.1$ cP for mAb 4 and 12.9 ± 0.1 cP for mAb 6). Further examination of light and heavy sequences of the four mAbs (mAb numbers 4, 6, 10 and 11) showed that differences among the two sets of mAbs could be localized to the framework regions and complementarity determining regions (CDRs) in the Fv portions.

There is also no correlation between viscosity at high concentration and pI value of a full length mAb. The pI values for all 11 mAbs were measured using cIEF experiments described in the Materials and Methods section. The pI values for mAbs 10 and 11 are 7.2 and 6.9, respectively. These values are approximately 1 to 1.5 units away from the formulation buffer pH (5.8), and are lower than typical pI values seen for mAbs in our experience. This prompted us to examine if a low value of pI of a mAb or relatively small difference between pI and the pH of the formulation buffer is indicative of its poor concentration dependent viscosity behavior. The pI values for mAb 7 and mAb 8 are 6.9 and 7.0, respectively. These are similar to the pI values of mAbs 10 and 11. However, both mAbs 7 and 8 demonstrate low viscosities at high concentrations. The solution viscosity of mAb 7 at 150 mg/ml is 13.9 ± 0.5 cP and the corresponding viscosity value for mAb 8 is 14.5 ± 1.1 cP (Table I). A linear regression between solution viscosities at 150 mg/mL for 11 mAbs and their measured pI values yielded an r^2 value of 0.29 and p-value of 0.09, thereby, accepting the null hypothesis that pIs and solution viscosities of the 11 mAbs at high concentrations are not statistically correlated. For rejecting the null hypothesis at 95% level of confidence, p-values should be below 0.05 [43]. Therefore, low pI for the whole mAb or its closeness to the formulation buffer pH does not always lead to poor concentration dependent viscosity behavior.

In summary, simple 'rules of thumb' based on properties of the whole mAbs such as pI and isotypes, that may be expected to be capable of identifying viscosity challenged mAb candidates, do not work consistently.

Observations from Concentration Dependent Viscosity Curves of 11 mAbs

The concentration dependent viscosity behavior of a solute can be described by Eqs. 1–3 in the Materials and Methods.

In particular, specific viscosity of a solute measures contribution of the solute towards the viscosity of the solution (Eq. 3). If there are no solute: solute interactions, the contributions from higher order terms in Eq. 3 are zero, resulting in a linear dependence of specific viscosity on solute concentration (see pages 434–435 in Creighton [36]). However, it is known that large proteins such as mAbs can significantly alter solution viscosity. Molecular crowding and excluded volume effects in highly concentrated antibody solutions lead to a non-linear dependence of specific viscosity on mAb concentration [44]. In addition to these effects, electrostatic complementarities, hydrophobic inter-molecular interactions and proximal energies [30] can also contribute towards non-linearity of concentration dependent viscosity curves of antibodies. Figure 1a compares viscosity behaviors of the 11 antibodies by plotting η_{sp}/c *versus* c. All curves in Fig. 1a eventually become nonlinear as the mAb concentrations increase, pointing to the importance of mAb: mAb inter-molecular interactions in all antibody solutions. Figure 1a also shows that the specific viscosities for mAbs 10 and 11 rise significantly faster than those for other mAbs. To compare rates of increase in viscosities for the 11 mAbs in this study upon increase in their concentration, the data in Table I was manipulated according to Eq. 2 and converted into linear plots shown in Fig. 1b *via* least squares fits to the following equation:

$$\eta_{rel} = Ae^{Bc} \tag{6}$$

Or,

$$\ln\eta_{rel} = \ln A + Bc \tag{7}$$

Where, η_{rel} is the relative viscosity [45] of a mAb at concentration c, computed by using Eq. 2. For each mAb, values of the intercept (lnA), slope (B), square of linear correlation coefficient (r^2) and statistical significance (p-values) are shown in Table II. Antilog of the intercept, A, is intrinsic relative viscosity [η_{rel}] of a mAb. The slope (B-value) measures the rate of increase in relative viscosity of a mAb with increase in its concentration [7]. Fig. 1b shows that all mAbs, except mAb11, have similar intercept values. This implies that intrinsic viscosities [η_{rel}] of these mAbs in infinitely dilute solutions are similar. However, the B-values (slope) are different for each mAb. In particular, the B-values for mAbs 10 and 11 are significantly greater than those for the remaining nine mAbs (Table II). This reflects significantly greater rate of increase in viscosity with concentration for mAbs 10 and 11 compared to mAbs 1–9. Since all mAbs in this study have similar general size and shape, it is reasonable to infer that the differences in their viscosity behaviors potentially result from the differences in their self-association properties. This observation is in agreement with the previous studies [1, 7, 12].

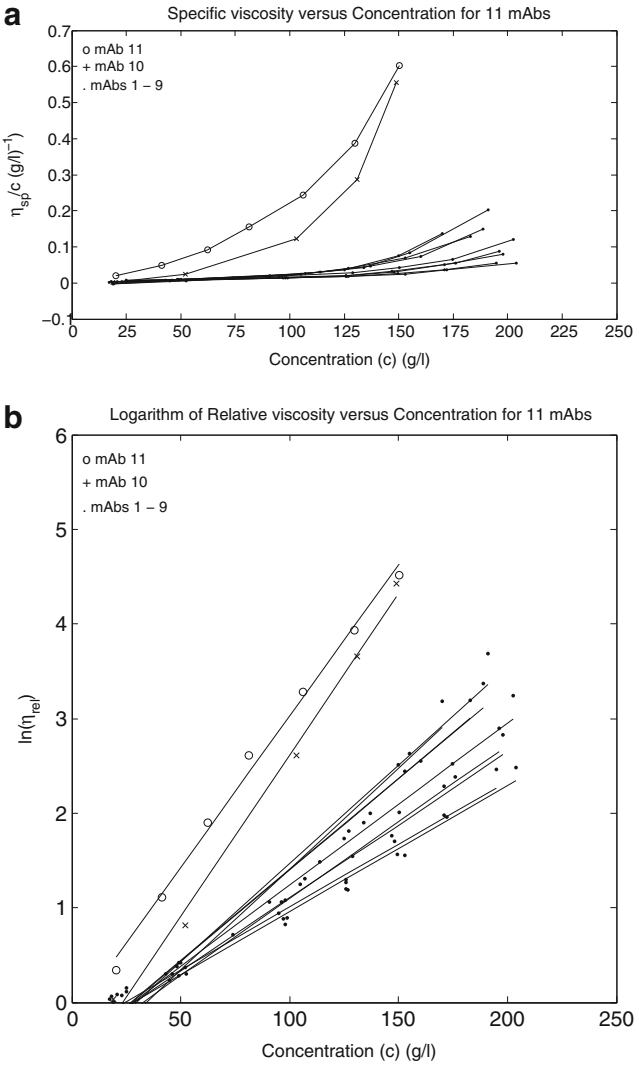

Fig. 1 (**a**) Concentration dependent viscosity curves for all 11 mAbs measured under identical experimental conditions. X-axis shows mAb concentration, c. Y-axis shows specific viscosity normalized by concentration (η_{sp}/c). Note that nine of the 11 mAbs in our dataset show low viscosities even at high concentrations. (**b**) Linear regression lines for concentration dependent viscosity data. Relationship between viscosity and concentration is logarithmic for all 11 mAbs and can be characterized using Eq. 7 in the text. η_{rel} and c are relative viscosity and concentration, respectively. The slope (B) and intercept (lnA) of these least squares fits are presented in Table II.

Correlating High Concentration Viscosity With Molecular Properties of Human Antibody Domains/Regions: Constructing Fv Region Profiles

Concentration dependent viscosity behavior of an antibody is a function of its ability to self-associate, and, therefore, must arise from molecular properties, such as net charge (Z), apparent charge (Z_{app}), ξ-potential, dipole moment, pI and

Table II Parameters for Logarithmic Relationship Between Relative Viscosity ($\ln(\eta_{rel})$) and mAb Concentration (c)*

mAb Number	lnA	A	B	r^2	p-value
1	−0.3699	0.6908	0.0133	0.98	9.9×10^{-6}
2	−0.3218	0.7248	0.0133	0.98	3.1×10^{-5}
3	−0.4375	0.6456	0.0154	0.97	4.2×10^{-5}
4	−0.5321	0.5874	0.0163	0.97	4.1×10^{-5}
5	−0.4749	0.6219	0.0171	0.98	2.4×10^{-6}
6	−0.5268	0.5905	0.0193	0.98	1.5×10^{-4}
7	−0.7256	0.4840	0.0213	0.96	4.9×10^{-4}
8	−0.5198	0.5946	0.0192	0.98	2.6×10^{-5}
9	−0.6147	0.5408	0.0208	0.96	5.1×10^{-4}
10	−0.7847	0.4563	0.0341	0.99	2.3×10^{-4}
11	−0.1707	0.8431	0.0320	0.99	8.7×10^{-6}

* Concentration dependent viscosity profiles shown in Fig. 1 were fitted with eq. 6 *via* linear regression. Values of lnA and B represent intercept and slope for each mAb respectively. The r^2 values indicate the correlation coefficients and p-values indicate the probability of accepting the null hypothesis that logarithmic relationship between relative viscosity and concentration is by random chance. The p-values below 0.05 are considered significant at 95% level of confidence [43]. The poorly behaved mAbs 10 and 11 have substantially greater slope (B-values) indicating that viscosities of these mAbs rise faster than other mAbs as the concentration increases.

hydrophobicity of the mAb and of the individual domains/regions in the mAb. By examining the molecular properties of individual structural domains in antibodies, one can estimate the nature of colloidal interactions formed by different antibody domains. A full length mAb contains 12 different structural domains (2 copies for each of V_L, C_L, V_H, C_H1, C_H2, and C_H3 domains). Eight (2 copies each of C_L, C_H1, C_H2 and C_H3) of these 12 domains remain constant, while the other four domains constituting the two variable regions, Fv (V_H:V_L), change among different mAbs. Out of the 11 mAbs in this study, seven have heavy chains of IgG1 isotype. The heavy chains in two mAbs are of IgG2 isotype and the remaining two are of IgG4 isotype. For the light chains, seven are of κ isotype and four are of λ isotype. Here, the molecular properties of the constant domains found in heavy and light chains of different isotypes were computed using the following crystal structures obtained from PDB entries: 1HZH (IgG1κ, human b12 mAb, [37]), 4HAG (human IgG2 Fc, [46]), 4C54 (human IgG4 Fc, [47]) and 2MCG (human λ light chain, [48]).

Colloidal interactions involving only the constant domains of human antibodies are expected to be predominantly repulsive in the optimal formulation pH range (5.5–6.3) for high concentration mAb formulations [34]. These domains have positive net charges and positive ξ-potentials in this pH range. Table III describes the molecular properties for all structural domains of human IgG1κ mAb, 1HZH. The data shown in this table indicates that all domains in the human b12 mAb have overall positive net charge (Z) and ξ-potential values at the formulation pH (5.8) in absence of salt. In particular, note that each domain in the constant regions including the hinge region has positive net charge (Z) at the formulation pH (5.8). Figure 2 shows the titration curves of net charge (Z) with respect to pH for each constant domain in 1HZH. It can be seen that all constant domains are significantly positively charged in the pH range 5.5–6.3. This is because pI values of the constant domains in b12 mAb are ≥7 (Table III). The net charge (Z) on whole mAb minus the Fv regions (that is, taking all constant regions together) is also positive along with positive ξ-potential ($Z_{\text{constant regions}}=+25.4$ and $\xi_{\text{constant regions}}=+89.4$ mV, Table III) at pH 5.8. The molecular properties were also computed for constant domains in the other heavy and light chain isotypes, namely, human IgG2 Fc, human IgG4 Fc and C_L domain from a human λ light chain (Table IV). All these constant domains, except for the C_H3 domains in IgG4 Fc, have overall positive net charges and positive ξ-potentials at pH 5.8 because their pI values are ≥6.5. Note that re-engineering of the Fc region for eliminating or enhancing Fc-mediated functions [49, 50] may alter the electrostatic properties of the constant domains. However, the impact of Fc-engineering on molecular properties of the constant domains was not studied here.

From the above observations, it is reasonable to expect that characteristics of variable regions significantly influence concentration dependent viscosity behavior of the full length mAbs, and thus may be useful for identifying mAb candidates with potential for high viscosity. The calculated electrostatic properties for the Fv regions of the 11 mAbs are shown in Table V, and Fig. 3a-d show solution viscosities for 11 mAbs plotted with respect to Z_{Fv}, ξ_{Fv}, pI_{Fv} and D_{Fv}. Note that isolated Fv regions of the 11 mAbs were neither produced nor experimentally studied in this work. Table V and Fig. 3a-d demonstrate that large negative values for Z_{Fv} and ξ_{Fv} could be symptomatic of increased viscosity at high concentration in antibody solutions. The Fv regions of both mAb 10 and mAb 11, which show high viscosity values at 150 mg/mL, have large negative values for Z_{Fv} and ξ_{Fv}. There is no added salt in the formulation buffer and the mAb samples were extensively dialyzed to minimize the counter-ions carried over from the purification train. In the modeling work, residual counter-ions were accounted for by computing apparent charges on the Fv regions (Z_{appFv}) at an arbitrarily chosen salt concentration (1 mM NaCl, low ionic strength). The magnitudes of apparent charge on the Fv portions of the 11 mAbs were found to be smaller than the magnitudes of the corresponding net charges ($|Z_{appFv}| < |Z_{Fv}|$ for all the Fv regions). However, signs (positive or negative) and overall trends remained the same (Table V). Interestingly, dipole moments of the Fv regions (D_{Fv}) are not correlated with the mAb viscosity values at 150 mg/mL (Fig. 3d). Dipole moment can be interpreted as overall distribution of charges in a molecule

Table III Calculated Protein Properties for Human b12 IgG1κ mAb and its Various Components at pH 5.8*

1HZH component	Average Net charge (Z)	ξ-potential (mV)	Isoelectric point (pI)	KD hydromom	Hydrophilic Van der Waals surface area (Å^2)	Hydrophobic Van der Waals surface area (Å^2)
Whole mAb	45.0 (46.2)	163.4 (167.6)	9.1 (9.2)	3,689.1 (3,603.8)	21,533.6 (21,399.1)	28,775.2 (28,605.2)
V_H chain H	2.9	9.8	8.7	540.2	2,860.7	3,839.5
V_H chain K	2.6	8.8	9.0	562.7	2,698.4	3,890.7
V_L chain L	7.2	24.0	9.6	295.4	2,309.7	3,161.0
V_L chain M	7.2	24.2	9.7	298.1	2,278.3	3,055.0
1HZH minus Fv regions	25.4 (25.8)	89.4 (90.8)	8.5 (8.6)	3,090.3 (3,019.9)	14,345.5 (14,042.2)	19,769.2 (19,671.2)
Fv1 (HL)	9.7	32.7	9.7	443.1	4,282.8	5,637.7
Fv2(KM)	8.8	29.5	9.8	462.8	4,135.8	5,669.3
Fab1 (HL)	18.8	63.9	9.4	721.4	7,220.7	9,459.1
Fab2 (KM)	16.3	55.4	9. 7	747.3	7,074.1	9,578.4
C_L chain L	0.9	2.9	7.0	184.1	2,549.5	3,247.2
C_L chain M	1.0	3.5	7.3	172.0	2,369.9	3,389.8
C_H1 chain H	5.5	18.4	9.8	290.0	2,000.9	3,371.2
C_H1 chain K	5.2	17.3	9.9	318.0	1,897.5	3,189.3
Hinge region	2.0	6.7	7.7	152.7	930.4	2,025.2
Fc	10.5 (10.7)	35. 8 (36.5)	7.9 (8.0)	1,523.6 (1,495.0)	7,901.3 (7,673.5)	11,052.8 (10,814.6)
C_H2 chain H	3.7 (3.6)	12.4 (12.0)	8.6 (8.8)	215.9 (185.2)	2,147.0 (2,223.7)	4,239.3 (4,293.4)
C_H2 chain K	3.7 (3.7)	12.5 (12.5)	8.6 (8.6)	284.0 (267.3)	2,240.9 (2,173.0)	4,208.5 (4,201.4)
C_H3 chain H	1.9	6.5	7.1	462.1	2,624.7	3,422.7
C_H3 chain K	2.0	6.7	7.3	408.4	2,516.7	3,480.5

*Values in parentheses were computed for whole mAb (human b12 mAb, PDB entry: 1HZH) and its components with their glycans removed. The crystal structure of this mAb has missing atomic coordinates and a broken inter-heavy chain disulfide bond. These were modeled in using MOE from Chemical Computing group (www.chemcomp.com) before performing the above calculations. The molecular properties were calculated for pH 5.8 and 0.001 M salt using protein properties module in MOE2012.10. Prior to these calculations, the N- and/or C-termini of each domain or component were neutralized *via* acetylation or amidation to mimic their state in the whole mAb. Each domain/component was also protonated at pH 5.8 and zero salt using Protonate3D module in MOE2012.10 and energy minimized. The following describe the residues included in each domain/component: V_H(Gln1-Ser127 in heavy chain H or K), V_L(Glu1-Lys108 in light chain L or M), C_L(Arg109-Cys215 in light chain L or M), C_H1(Ala128-Ala225 in heavy chain H or K), Hinge(Glu226-Pro240 from both the heavy chains H and K), C_H2(Ala241-Lys350 in heavy chain H or K), C_H3(Gly351-K457 in heavy chain H or K), Fc (Ala241-Lys457 in heavy chains H and K with or without glycans), Fab (Gln1-Cys230 and Glu1-Cys215 in heavy and light chain pairs HL or KM), Fv (Gln1-Ser127 and Glu1-Lys108 in heavy and light chain pairs HL or KM), 1HZH minus Fv regions (Ala128-Lys457 and Arg109-Cys215 in heavy and light chain pairs HL and KM with or without glycans). The pI values were computed using the atomic coordinates. KDhydromom is Kyte-Doolittle hydrophobicity moment.

and Dipole moment of the whole mAb ($D_{\text{whole mAb}}$) is likely to be more relevant to high concentration viscosity than that of the Fv only (D_{Fv}).

For the 11 mAbs in this study, the macromolecular tendency to exclude solvent (hydrophobicity) may be less relevant compared to the electrostatic interactions for reversible attractive self-associations among the antibody molecules. Table VI shows calculated hydrophobic properties of the Fv regions of the 11 mAbs. It can be seen that there are no clear correlations between high concentration viscosity values of the 11 mAbs with either hydrophobicity or aggregation propensities of their Fv regions. It remains to be seen if this observation will hold true, when experimental data becomes available on a larger number of antibody molecules.

Overall, the above data analyses indicate that the Fv regions of therapeutic mAb candidates can be classified into three broad electrostatic profiles (Figs. 4 and 5) that may qualitatively correlate with concentration dependent viscosity behavior of the whole mAb:

(i) Profile 1: Both Z_{Fv} and ξ_{Fv} are significantly positive (Fig. 4a, illustrated by blue colored titration curves in Fig. 5a and top row in Fig. 5b) in the optimal formulation pH range (5.5 – 6.3). Because of the additive nature of the net charge (Z) as well as ξ-potentials of the antibody domains, it can be safely estimated that $Z_{\text{whole mAb}} > Z_{\text{constant regions}}$ and $\xi_{\text{whole mAb}} > \xi_{\text{constant regions}}$ in such cases. This would make the whole mAb molecules more repulsive towards one another than the constant regions alone. In highly concentrated solutions of such antibodies, electrostatic repulsion and the tendency to exclude the solvent (hydrophobicity) would work at cross purposes, and the overall self-interactions would be repulsive until the mAb solubility limit is reached. Fv portions of 7 mAbs in this

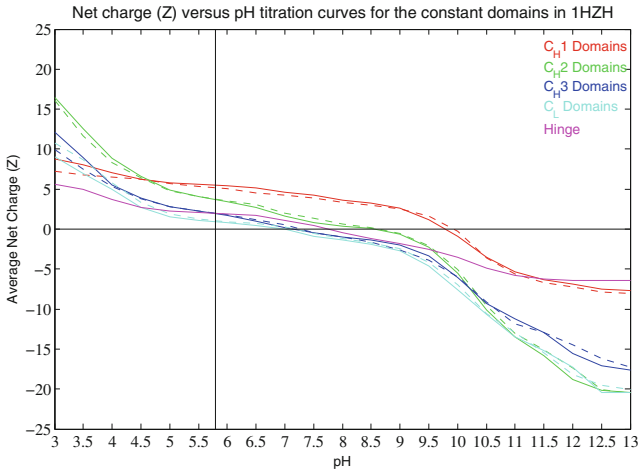

Fig. 2 Calculated Net charge (Z) *versus* pH titration curves for the individual constant domains in a human IgG mAb. X-axis indicates the pH and Y- axis indicates the calculated Net charge (Z). These calculations were performed using the atomic coordinates of individual domains extracted from 1HZH crystal structure and the Protein Properties module in MOE2012.10. Each domain structure was protonated at pH 5.8, zero salt concentration and energy minimized. See materials and methods for more details. Continuous and dashed lines of the same color show the titration curves for the same domain in both the heavy or light chains. For example, continuous and dashed red lines indicate the titration curves for C_H1 domains from the heavy chains H and K in 1HZH structure. Note that all constant domains have positive net charge (Z) in the commonly used formulation pH range (5.5 – 6.3). Therefore, inter-molecular interactions among the mAbs that involve only the constant regions are expected to be predominantly repulsive.

dataset follow Profile 1 (Table V) and two of them, mAb1 and mAb 2, are shown in the top row of Fig. 5b.

(ii) Profile 2: Z_{Fv} may be close to zero and ξ_{Fv} may have low magnitude (Fig. 4b, illustrated by green colored titration curves in Fig. 5a and the middle row in Fig. 5b) in the optimal formulation pH range (5.5–6.3). In such cases, $Z_{\text{whole mAb}} \sim Z_{\text{constant regions}}$ and $\xi_{\text{whole mAb}} \sim \xi_{\text{constant regions}}$ and electrostatic repulsions among the mAb molecules mainly arise from their constant regions. Hydrophobicity and mAb structural features such as shape complementarities are expected to play greater role in determining the tendency for inter-molecular interactions among the mAbs whose Fv regions follow this second profile. The low charge on the Fv portions could be due to either large hydrophobic patches or mutual cancellation between positively and negatively charged patches. Both of these cases (mAbs 5 and 7) were found in the dataset of 11 mAbs (the middle row in Fig. 5b). High concentration solutions of both these mAbs show low viscosities. Measured viscosities of mAb 5 and mAb 7 solutions at 150 mg/mL are 8.4±0.1 cP and 13.9 ±0.5 cP, respectively. At this time, there are only two molecules in our study that follow the Profile 2. Therefore, it is unclear if highly concentrated solutions of Profile 2 mAb candidates shall always show low viscosities. More examples are needed to derive overall rules with respect of the viscosity behavior of mAbs whose Fv regions follow Profile 2.

(iii) Profile 3: Z_{Fv} and ξ_{Fv} are significantly negative (Fig. 4c, illustrated by red colored titration curves in Fig. 5a and the bottom row in Fig. 5b) in the optimal formulation pH range (5.5–6.3). This situation would lower Z and ξ-potential on the whole antibody resulting in $Z_{\text{whole mAb}} < Z_{\text{constant regions}}$ and $\xi_{\text{whole mAb}} < \xi_{\text{constant regions}}$ and

Table IV Calculated Protein Properties for Constant Domains Found in non- IgG1κ mAbs at pH 5.8*

Constant domain/region in human mAbs	Average Net charge (Z)	ξ-potential (mV)	Isoelectric point (pI)	KD hydromom	Hydrophilic Van der Waals surface area (Å^2)	Hydrophobic Van der Waals surface area (Å^2)
C_L domain (G111-S216) from λ LC in 2MCG.1	2.9	9.7	8.1	198.7	3,380.5	2,175.8
IgG2 Fc dimer from 4HAG (G237-S444 in each HC)	8.3 (8.2)	28.4 (28.1)	7.4 (7.5)	1,009.5 (972)	7,835.8 (7,700.2)	10,803.2 (10,799.0)
IgG2 Fc C_H2 domain (G237-K340) in HC 1	3.6 (3.7)	12.0 (12.5)	8.6 (8.6)	109.8 (123.1)	2,124.6 (2,070.8)	3,768.1 (3,806.5)
IgG2 Fc C_H2 domain (G237-K340) in HC 2	3.6 (3.6)	12.2 (12.0)	8.6 (8.6)	107.7 (127.5)	2,062.4 (2,031.4)	3,794.6 (3,786.0)
IgG2 Fc C_H3 domain (G341-S444) in HC 1	1.0	3.3	6.5	376.4	2,611.1	3,245.6
IgG2 Fc C_H3 domain (G341-S444) in HC 2	0.9	2.9	6.5	385.1	2,607.9	3,299.4
IgG4 Fc dimer from 4C54 (G237-S444 in each HC)	2.2 (2.2)	7.4 (7.5)	6.5 (6.5)	604.4 (643.1)	8,037.3 (7,639.3)	10,835.0 (10,314.3)
IgG4Fc C_H2 domain (G237-K340) in HC A	2.6 (2.6)	8.8 (8.8)	8.7 (8.8)	231.1 (240.9)	2,280.2 (2,201.0)	3,751.4 (3,726.7)
IgG4Fc C_H2 domain (G237-K340) in HC B	2.6 (2.6)	8.7 (8.8)	8.7 (8.6)	219.7 (211.1)	2,168.0 (2,085.7)	3,807.2 (3,886.0)
IgG4 Fc C_H3 domain (G341-S444) in HC A	−1.2	−3.9	5.0	379.5	2,457.4	3,348.6
IgG4 Fc C_H3 domain (G341-S444) in HC B	−1.1	−3.7	5.0	404.2	2,453.2	3,314.8

* Values in parentheses are for human IgG2 and IgG4 Fc regions and C_H2 domains with their glycans removed. The crystal structures used in this calculations are 2MCG (human λ light chain), 4HAG (human IgG2Fc) and 4C54 (human IgG4 Fc). The domains were extracted from the crystal structures and optimized before performing the above calculations. These properties were calculated for pH 5.8 and 0.001 M salt using protein properties module in MOE2012.10. Prior to these calculations, the N- and/or C-termini of each domain or component were neutralized *via* acetylation or amidation to mimic their state in the whole mAb. Each domain/component was also protonated at pH 5.8 and zero salt using Protonate3D module in MOE2012.10 and energy minimized. The pI values were computed using the atomic coordinates. KDhydromom is Kyte-Doolittle hydrophobicity moment.

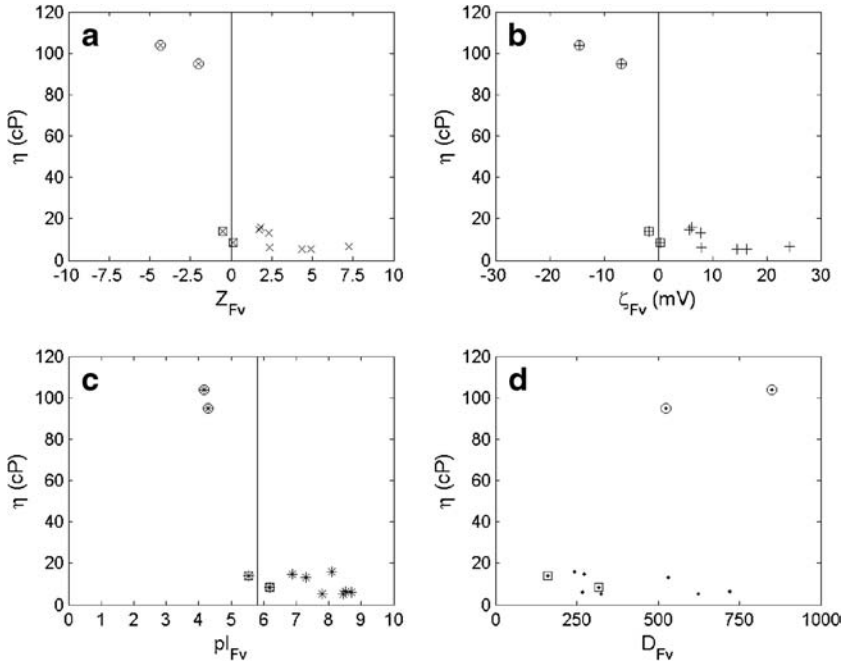

Fig. 3 High concentration (~150 mg/mL) viscosity (η) values of 11 mAbs plotted with respect to the electrostatic properties of their Fv regions, namely, Z_{Fv}, ξ_{Fv}, pI_{Fv} and D_{Fv}. In each plot, X-axis represents an electrostatic property of the Fv regions and Y-axis represents solution viscosity (η) of the whole mAb at approximately 150 mg/mL. The data points for mAbs 10 and 11 (Profile 3) are circled. Note that Fv regions of these mAbs have significantly negative Z_{Fv} and ξ_{Fv} potential values at the formulation pH (5.8) in absence of salt. The values of pI_{Fv} are below formulation pH for these mAbs. The data points for mAbs 5 and 7 (Profile 2) are boxed. These mAbs show low values for Z_{Fv} and ξ_{Fv} at the formulation pH (5.8) in absence of salt. Their pI_{Fv} values are also close to the formulation pH as seen in η *versus* pI_{Fv} plot. The remaining seven data points are for the Fv regions belonging to Profile 1 (significantly positive Z_{Fv} and ξ_{Fv}).

Table V Calculated Electrostatic Molecular Properties of the Fv Portions of the 11 mAbs*

mAb #	η(cP) at ~150 mg/mL	Z_{Fv}	Z_{appFv}	ξ_{Fv} (mV)	pI_{Fv}	Profile type
1	5.4±0.1	4.3	1.4	14.6	7.8	1
2	5.4±0.1	4.9	1.6	16.4	8.4	1
3	6.2±0.1	2.4	0.8	8.0	8.7	1
4	6.6±0.1	7.2	2.4	24.3	8.5	1
5	8.4±0.1	0.1	0.0	0.4	6.2	2
6	12.94±0.1	2.3	0.8	7.8	7.3	1
7	13.94±0.5	−0.5	−0.2	−1.7	5.5	2
8	14.54±1.1	1.7	0.6	5.8	6. 9	1
9	15.64±0.6	1.8	0.6	6.1	8.1	1
10	94.74±0.6	−2.0	−0.7	−6.8	4.3	3
11	103.64±1.0	−4.3	−1.4	−14.6	4.2	3

* The calculations were performed using the Protein Properties module in MOE2012.10. The symbol η denotes the measured viscosity of the antibody solution at the target concentration of 150 mg/mL. Z_{Fv}, Z_{appFv}, ξ_{Fv} and pI_{Fv} are calculated values of net charge, apparent charge, ξ potential, and pI of the Fv portions, respectively. Z_{Fv}, Z_{appFv} and ξ_{Fv} were calculated at pH 5.8 and 1 mM NaCl (low ionic strength). Note that these mAbs, with poor concentration dependent viscosity behaviors, have negative values for Z_{Fv}, Z_{appFv} and ξ_{Fv}. Furthermore, their calculated pI_{Fv} values are lower than the formulation pH.

would enhance the electrostatic polarization within an antibody structure. In this scenario, local regions of charge complementarities allow more frequent close encounters and self-associations at high concentrations. For mAbs whose Fv regions fall in this third profile, electrostatic features of Fv region may work in tandem with hydrophobicity to promote proximal attractive intermolecular interactions. Highly concentrated solutions of such mAbs are expected to show high viscosities, even though the overall $Z_{\text{whole mAb}}$ and $\xi_{\text{whole mAb}}$ may still be positive. In the dataset of 11 mAbs studied here, the Fv portions of mAb 10 and mAb 11 follow Profile 3 (Table V). The calculated pIs of the Fv regions of these two mAbs are also below 5.8, the pH of the formulation buffer (pI_{Fv}=4.3 for mAb 10 and 4.2 for mAb 11). The bottom row in Fig. 5b shows electrostatic surfaces for these Fv portions. The negative charges on Fv surface may either be concentrated into large patches or be distributed all over the Fv surface. Both the cases were observed here (Fig. 5b). Currently, there are only two mAbs with this type of concentration dependent viscosity behavior in our dataset. Nonetheless, consistent with the above rationale, values of the interaction parameter measured by DLS experiments were found to be negative in the pH range 5.0–6.0 for mAb10 and mAb11 (data not shown), indicating attractive self-association.

Table VI Calculated hydrophobic molecular properties of the Fv portions of the 11 mAbs

mAb #	η(cP) at ~150 mg/mL	$P_{agg}TANGO_{Fv}$*	$P_{agg}WALTZ_{Fv}$*	H_{Fv}*	KD $hydromom_{Fv}$*	$HpASA_{Fv}(Å^2)$*
1	5.4 ± 0.1	4.9	5.0	25.9	559.0	23.3
2	5.4 ± 0.1	2.5	3.9	26.7	369.4	23.3
3	6.2 ± 0.1	3.3	8.5	25.1	475.3	24.3
4	6.6 ± 0.1	4.6	8.2	25.3	541.8	24.4
5	8.4 ± 0.1	7.3	3.2	25.9	577.3	23.2
6	12.9 ± 0.1	2.8	6.2	24.4	494.7	23.1
7	13.9 ± 0.5	4.0	5.5	25.4	312.3	23.5
8	14.5 ± 1.1	4.0	7.7	26.7	443.5	24.7
9	15.6 ± 0.6	9.7	10.5	25.8	455.1	25.1
10	94.7 ± 0.6	4.2	7.6	24.6	344.9	23.2
11	103.6 ± 1.0	1.7	9.8	25.0	592.6	25.1

* $P_{agg}TANGO_{Fv}$ and $P_{agg}WALTZ_{Fv}$ are normalized TANGO/WALTZ aggregation propensities. H_{Fv} is normalized hydrophobicity and $HpASA_{Fv}$ is normalized hydrophobic surface area values. These values were calculated as described in materials and methods. KD $hydromom_{Fv}$ is Kyte-Doolittle hydrophobicity moment. Hydrophobic surface area and K-D hydrophobicity moment were computed from structural models of the Fv regions using the Protein Properties module in MOE2012.10. The hydrophobic molecular properties of the Fv portions of 11 mAbs do not correlate with viscosity at high concentration.

In all three of the above Fv region profiles, the overall extents of electrostatic and hydrophobic effects depend on individual sequence and structural properties of the mAbs as well as the buffer conditions. Therefore, concentration dependent viscosity behaviors of mAbs in all the three profiles could vary considerably on a case to case basis. Furthermore, these profiles do not take into account the impact salt may have on the viscosity.

Attractive Self- Association Slows the Diffusion of Antibody Molecules: Insights from Coarse-Grained Simulations

Coarse-grained simulations can help with understanding differences in the solution behavior of mAbs. Here, such simulations were performed on three mAbs, namely, mAb 1 (Profile 1, low solution viscosity at high concentration), mAb 10 and mAb 11 (Profile 3, high solution viscosity at high concentrations) at 300 K and at low (30 mg/mL) and high (100 mg/mL) concentrations.

The two high viscosity mAbs, mAb 10 and mAb 11 were found to diffuse slower than a well-behaved mAb (mAb1) at both concentrations. From the coarse-grained simulations of mAb 1, performed at 300 K and concentration of 30 mg/mL, linear fit of mean squared displacement ($<x^2>$) *versus* time (t) resulted in an estimated diffusion coefficient (D) at 1.63 $Å^2$/ns (= 1.63 × 10^{-7} cm^2/s). Similarly, from simulations performed under the same conditions diffusion coefficients were estimated at 0.86 $Å^2$/ns and 0.42 $Å^2$/ns for mAbs 10 and 11 respectively. These values have the same order of magnitude as the experimental values reported by Saltzman and coworkers for infinitely dilute solutions of human Immunoglobulins [51]. Furthermore, these coarse-grained simulations were able to reproduce the trends seen from the experimental data. Higher diffusion coefficients correspond to lower viscosities as would be expected from the Stokes-Einstein equation (Materials and Methods). The differences in the estimated diffusion coefficients of mAbs 10 and 11, compared to mAb 1, suggest that coarse-grained simulations of antibodies with the same general Fv region electrostatic surface properties as the mAbs in this study, can qualitatively recapitulate the observed differences in their experimentally determined viscosity behavior. The decreasing trend in translational diffusivity can be attributed to an increasing trend in their attractive self-association behavior, due to the increasing electrostatic complementarities between their Fab and Fc fragments. In simulations performed at 100 mg/mL, the increased molecular crowding decreases overall diffusivities of the mAbs approximately ten-fold, compared to those at 30 mg/mL. The estimated diffusion coefficients for mAbs 1, 10 and 11 were 0.097, 0.062, and 0.045 $Å^2$/ns, respectively, in the simulations performed at 100 mg/mL and 300 K. In spite of the general dampening of molecular motions, it is interesting to observe that the electrostatic complementarity differences among the mAbs arising due to the differences in net charges of their Fv regions, were able to again recapitulate the general viscosity trends for these mAbs. The coarse-grained simulations performed here confirm that molecular crowding [44] and charge on the Fv regions, both, play important roles in determining concentration dependent viscosity behaviors for mAbs 1, 10 and 11.

Can Fv Region Molecular Properties Quantitatively Predict Viscosity of a Highly Concentrated mAb Solution?

Availability of self-consistent experimental viscosity data on 11 mAbs has afforded us an opportunity to explore the feasibility of quantitatively predicting viscosity of a highly concentrated

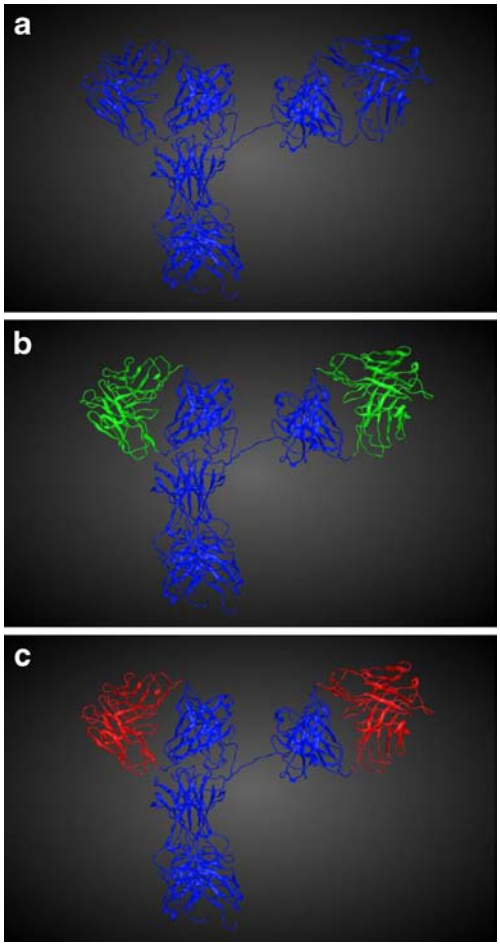

Fig. 4 Schematic diagrams showing different electrostatic profiles for Fv regions in mAbs (**a**) Profile 1: All domains in the mAb, including the Fv regions, show positive net charge (Z) and ξ-potential at formulation pH in absence of salt. All structural domains of the mAb are shown in blue colored ribbons to indicate their overall positive charge. (**b**) Profile 2: Net charge and ξ-potential for the Fv region (Z_{Fv} and ξ_{Fv}) ~ 0 at formulation pH in absence of salt. In this case, the Fv portions of the mAb are shown in green ribbons while the constant regions are shown in blue color. (**c**) Profile 3: Z_{Fv} and ξ_{Fv} are negative at formulation pH in absence of salt. In this case, the Fv portions of the mAb are shown in red ribbons while the constant regions are shown in blue color.

mAb solution using molecular descriptors calculated from its Fv region. All the electrostatic and hydrophobic parameters calculated from the molecular models of the Fv portions of 11 mAbs (see data in Tables V and VI) were explored for predicting values of natural logarithm of the relative viscosity ($\ln(\eta_{rel})$) at 150 mg/mL mAb concentration. For each mAb, $\ln(\eta_{rel})$ at 150 mg/mL was calculated using Eq. 7 and the slope and intercept values shown in Table II. The best regression model obtained from mathematical modeling is shown in the Eq. 8.

$$\frac{\ln(\eta_{rel})}{Nres_{Fv}} = 0.022182 - 0.55131 \times \left(\frac{pI_{Fv}}{Nres_{Fv}}\right) + 0.00087416 \times \left(\frac{P_{agg}Waltz_{Fv}}{Nres_{Fv}}\right) \quad (8)$$

Where, $\ln(\eta_{rel})$ is natural logarithm of relative viscosity values for the mAbs at 150 mg/mL, pI_{Fv} is the structure based pI calculated from molecular structure models of the Fv regions, $P_{agg}Waltz_{Fv}$ is sequence based aggregation propensity computed, using Waltz [40] for the residues in Fv regions, and $Nres_{Fv}$ is number of residues in the Fv regions. Normalization by $Nres_{Fv}$ removes potential biases due to size differences among the Fv regions of different mAbs. Plotting the predicted and experimentally determined values of $\ln(\eta_{rel}/Nres_{Fv})$ yielded an r^2 of 0.93 and, from Fig. 6, it can be seen that most of the data points fall within the 95% level of confidence. Goodness of fit as measured by root mean square error (RMSE) for predicted *versus* experimental values of $\ln(\eta_{rel}/Nres_{Fv})$ is 1.32×10^{-3} and the p-value is 1.91×10^{-5}, indicating high statistical significance for this relationship. This regression (Eq. 8) was repeated 11 times on 10 mAbs that remained after leaving out a mAb (Leave One Out analysis). A different mAb was left out each time. The relationship of normalized values of pI_{Fv} ($pI_{Fv}/Nres_{Fv}$) and aggregation propensity ($P_{agg}Waltz_{Fv}/Nres_{Fv}$) with $\ln(\eta_{rel})/Nres_{Fv}$ was found to be highly significant in all cases with p-values ranging from 9.3×10^{-6} to 3.5×10^{-4}. The r^2 values ranged from 0.88 to 0.96 and the RMSE values ranged from 1.01×10^{-3} to 1.41×10^{-3}. These observations imply that high concentration viscosity for an antibody may be predictable from pI and aggregation propensity values of its Fv region, using correlations derived from a training set of antibodies where all measurements have been performed under consistent conditions.

The origins of the two parameters in the Eq. 8, namely, pI and aggregation propensity can be ultimately traced to electrostatic and hydrophobic properties that determine intermolecular interactions among the mAb molecules. From the observations made in previous sections, the electrostatic intermolecular interactions are dominant among the mAbs in this study. Consistently, Eq. 8 shows that pI plays a greater role in determining the value of $\ln(\eta_{rel})$ than aggregation propensity. This was confirmed by performing linear regressions of normalized relative viscosity ($\ln(\eta_{rel})/Nres_{Fv}$) with normalized pI_{Fv} ($pI_{Fv}/Nres_{Fv}$) and normalized aggregation propensity ($P_{agg}Waltz_{Fv}/Nres_{Fv}$) separately. The r^2 value for a linear correlation of $\ln(\eta_{rel})/Nres_{Fv}$ with $pI_{Fv}/Nres_{Fv}$ alone is 0.734. The p-value for this correlation is 7.55×10^{-4} and the RMSE value is 2.5×10^{-3}, implying a significant correlation between $\ln(\eta_{rel})$ and normalized pI_{Fv}. The relationship between these two is represented by Eq. 9:

$$\frac{\ln(\eta_{rel})}{Nres_{Fv}} = 0.028269 - 0.56424 \times \left(\frac{pI_{Fv}}{Nres_{Fv}}\right) \quad (9)$$

Therefore, a decrease in pI of the Fv region (pI_{Fv}) is correlated with increased viscosity of the mAb at high concentration. No correlation was observed between $\ln(\eta_{rel})/Nres_{Fv}$ and $P_{agg}Waltz_{Fv}/Nres_{Fv}$ alone for the mAbs studied

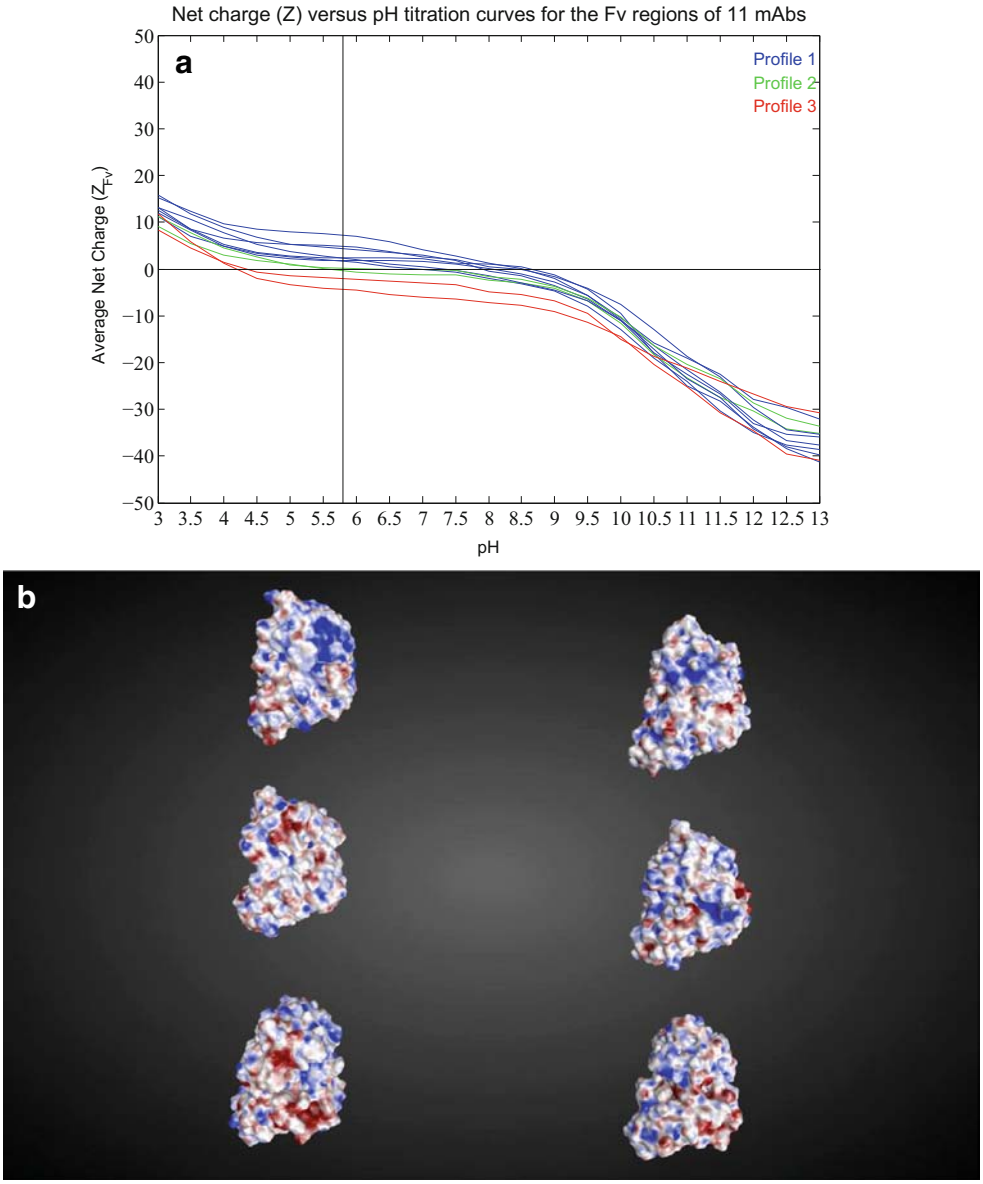

Fig. 5 (**a**) Net charge (Z) *versus* pH titration curves for the Fv regions of 11 mAbs in this study. The titration curves are colored according profiles of the Fv regions: Profile 1, blue; Profile 2, green; and Profile 3, red. (**b**) Examples of surface electrostatic maps for the Fv regions that fall in one of the three profiles described in the text and schematically depicted in the Fig. 4. Examples of Fv regions from mAb 1 and mAb 2 that follow Profile 1 are shown in the top row. In the middle row, the Fv regions from mAb 5 and mAb 7, that follow Profile 2, are shown. Fv regions from mAb 10 and mAb 11, that follow Profile 3, are shown in the last row at the bottom. In all the maps, increasing blue and red hues indicate increasingly positive and negative charges, respectively. All Fv regions were superposed on one another and oriented such that the antigen binding face is seen when looking down plane of the paper.

here. The concentration of 150 mg/mL was used here because experimental data show the greatest diversity around this concentration (Fig. 1a). This is also the highest concentration at which viscosity data is available for all mAbs in our data set (Table I). In principle, similar equations can be derived for other high concentrations as well. Viscosity of a mAb at 150 mg/mL, that was not included in the current dataset of 11 mAbs, could be correctly estimated using the above regression equations. Therefore, these correlations appear promising. However, they should be treated with caution because the number of mAbs in this dataset is small and there are only two mAbs that show high viscosities at increasing concentrations.

DISCUSSION

A major goal of this work was to find molecular properties that can be easily calculated from amino acid sequence and structural models (of the variable regions) of the antibodies and are capable of identifying therapeutic mAb candidates whose development as highly concentrated drug products may prove difficult. Such correlations could be valuable for developability risk assessments performed at early stages of drug discovery. It is feasible to 'red flag' mAb candidates, with potential of forming highly viscous solutions in high concentration formulations, using the profiles devised here. The molecular models of Fv portions of mAbs can be rapidly

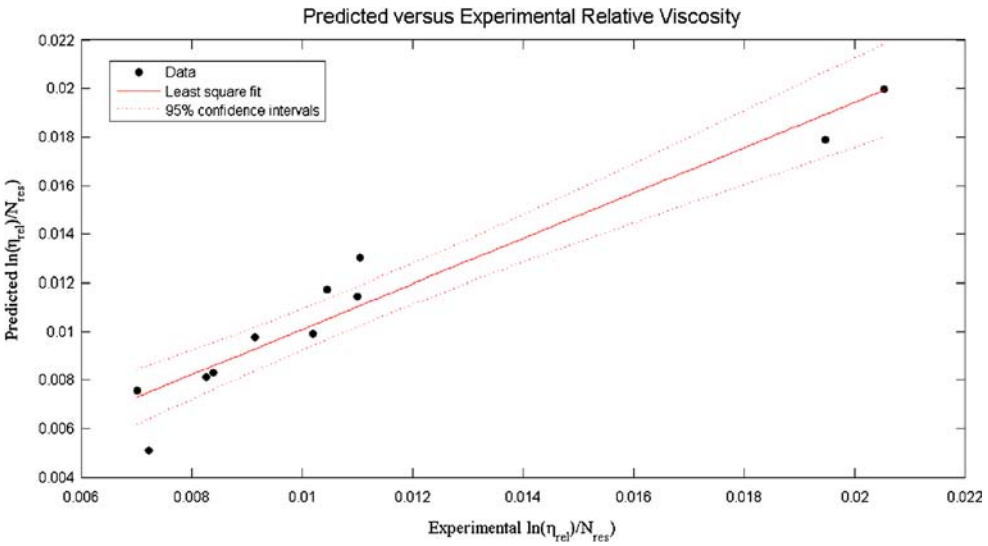

Fig. 6 Plot of predicted *versus* experimental values of ln (η_{rel}/$Nres_{Fv}$). The predicted values were calculated using the Eq. 8 derived from attempts to correlate molecular properties computed from sequences and structural models of Fv regions of the 11 mAbs with relative viscosity of the mAbs at 150 mg/mL.

constructed using commonly available software. Therefore, several affinity matured and humanized Fv constructs can be profiled *in silico*, in a high throughput manner, even before any materials are made or experiments are conducted. High risk candidates can be discarded or re-engineered in the discovery setting, before moving them into development. It must be noted that a level of false positives can be tolerated at this stage, but a false negative can result in enhanced development costs and possibly even failure to meet desired target product profiles.

In the literature, high concentration solution behaviors of one or two mAbs in different solution conditions have been compared [7, 12, 27, 28]. For example, Lileystrom *et al.* [7] have compared concentration dependent viscosity of two mAbs, showing opposite behaviors at high concentration, at different salt concentrations. The present study is complementary to the earlier studies and presents an orthogonal view. Here, concentration dependent viscosity measurements for all the 11 mAbs were carried out under identical solution conditions and by following identical experimental procedures. This strategy enables direct comparisons among different mAbs. The experimental results were supplemented with construction of molecular models of the Fv portions of the 11 mAbs using the same modeling software and procedures. Electrostatic and hydrophobic molecular descriptors calculated from the Fv models were correlated with the experimental viscosity data *via* mathematical modeling. Our findings on the significance of the Fv region were further corroborated by the observations from the coarse-grained molecular simulations performed on mAbs with poor (mAbs 10 and 11) and good (mAb 1) viscosity behaviors. The overall negative charge on the Fv regions of mAbs 10 and 11 facilitated attractive intermolecular interactions and self-associations that caused them to diffuse slower than mAb1 at both high and low concentrations.

There are several limitations to the work performed here. The parameters for solvation, pH and ionic strength were taken into account implicitly in molecular modeling calculations performed here. No parameters for excipients and formulation buffer components were included in the calculations. The native structure of antibodies can be destabilized at high mAb concentration [5, 24, 25], thereby, accelerating irreversible molecular self-association. This was also not explicitly modeled here, but was implicitly considered by computing sequence based aggregation propensities. These calculations also did not take into account characteristics of charge distribution and shape complementarities among solvent exposed charged patches and how these features contribute towards overall viscosity behavior of a mAb. An exploration of the above mentioned modeling limitations is deferred to future work. Contributions of hydrophobicity towards intermolecular interactions were less significant than the electrostatic interactions in this dataset of mAbs. However, this may change for other mAb datasets. Lastly, this study was also limited by the number of mAbs for which self-consistent experimental measurements are currently available. Our ongoing efforts aim to increase the number of mAbs in this dataset.

Despite the above mentioned challenges, the work presented here lays the foundation for predicting behavior of highly concentrated antibody solutions *via* correlations observed between the experimental data on full length mAbs and the molecular properties calculated using only their Fv regions. These correlations have confirmed our underlying hypothesis: Differences in highly concentrated antibody solution behaviors for the mAbs originate primarily from sequence-structural properties of their Fv regions. Moreover, it was feasible to create qualitative Fv molecular properties profiles capable of identifying problematic therapeutic candidates early on.

The structural architecture of the antibodies is modular in nature and therefore it is useful to consider the properties of constant and variable regions separately. The calculations reported here indicate that most of the constant domains in human antibodies have positive net charges and positive ξ-potentials in the typical pH range (5.5–6.3) used for formulation of high concentration therapeutic mAbs [34]. This is because the calculated pI values for all constant domains are ≥6.5, except for the C_H3 domain in IgG4 mAbs. Therefore, colloidal interactions involving only the constant domains of the mAbs should be predominantly repulsive in the high concentration mAb formulations. This study did not take into account impact of Fc engineering to enhance/eliminate Fc functions (FcγR, C1q or FcRN binding) [49, 50] on the electrostatic properties of the constant domains. However, this effect is expected to be small, given that most Fc-engineering mutations do not seek to significantly alter the overall Fc structure and molecular properties.

This work used calculated net charge (Z_{Fv}) for the correlation analyses. It is known that counter-ions bind proteins in a selective manner, thereby, modulating their charge and solution behavior [52, 53]. The values of charge computed from amino acid sequences for proteins do not take into account the effect of counter-ions and such estimates can differ substantially from the experimentally measured values. Lehermayr *et al.* [54] have experimentally measured net charge on 8 different mAbs at pH 6.0 in 20 mM His/His-HCl buffer *via* three different methods. The measured net charge values range between 6.8 and 22.5 depending upon the experimental method used by the authors, while the calculated values of net charge ranged from 18.5 to 40.0 (see Table II in Lehermayr *et al.*). However, it could be noted that the overall rank orders are very similar between calculated and experimentally measured charge values [54]. Laue has also shown that the charges calculated for mAbs from their sequences are linearly related to the Debye-Hückel Henry (DHH) charges that were deduced from experimental measurements. The sequence based calculated charge values for several full length mAbs were shown to be higher but rank-ordered similar to the DHH charges, both being positive at the pH values 5 and 6 [55]. In the present study, the values of net charge on Fv regions (Z_{Fv}), at the formulation buffer pH (5.8), were estimated by using their structural models rather than simply the amino acid sequences. Here, Z_{Fv} was computed by summing the partial charges on each atom in an Fv molecular model. This required accurate estimation of protonation states and pKa values of the amino acid residues in the Fv models. Local pH dependent protonation states of different residues can be rapidly estimated using PROPKA [56–58]. From the Fv models, it was also feasible to estimate apparent charge (Z_{appFv}) of an Fv region. Z_{appFv} is the apparent charge on an Fv at one Debye length. The Z_{appFv} values follow the same trends as Z_{Fv}, although their magnitudes are smaller. Therefore, it was immaterial whether Z_{Fv} was used instead of Z_{appFv} in construction of the Fv profiles. Note that no experimental charge measurements on the Fv portions of the 11 mAbs were performed in this study.

This work has improved our understanding of the impact of protein-protein interactions on solution behavior of the antibodies. This is a step towards rational design of mAbs for development as highly concentrated solutions suitable for subcutaneous delivery. Manipulation of the charged residues in the Fv regions can improve solution behaviors of highly concentrated antibody solutions. Consistent with the work of Shire and coworkers [22, 23] and the analyses reported here, neutralization of a negatively charged patch in FR3 region of the light chain of mAb10 *via* a single point mutation significantly improved its solubility and reduced viscosity at high concentration (our unpublished results).

CONCLUSIONS

Availability of concentration dependent viscosity data for several mAbs, obtained using standardized formulation and experimental procedures, enabled the correlation of their solution behaviors with molecular properties of their Fv regions. The Fv region profiles derived in this work can be used to rapidly screen therapeutic mAb candidates for their suitability towards high concentration formulation, in early stage drug discovery. While recognizing limitations due to a small dataset, this work represents a promising effort towards predicting viscosity behaviors of highly concentrated antibody solutions.

ACKNOWLEDGMENTS AND DISCLOSURES

Pfizer Business Technology is thanked for computational facilities. A postdoctoral fellowship to P.M.B. by Pfizer Inc. is gratefully acknowledged. Drs. Donna Luisi, David Sek, Norman MacDougall and Robert Walters are acknowledged for several constructive discussions and help with experiments. S.K. acknowledges his discussions with Joseph McLaughlin on viscosity measurements and data manipulations. All authors are employees of Pfizer Inc.

LL, CB, PN, NL, DB and JL performed the experiments. SK performed data analyses and PMB performed Coarse-grained simulations. LL and SK wrote most of the manuscript. SK and SKS conceived the concept of using molecular modeling to understand viscosity. All authors read and contributed towards improving the manuscript draft.

REFERENCES

1. Liu J, Nguyen MD, Andya JD, Shire SJ. Reversible self-association increases the viscosity of a concentrated monoclonal antibody in aqueous solution. J Pharm Sci. 2005;94:1928–40.
2. Johnsonand HR, Lenhoff AM. Characterization and Suitability of Therapeutic Antibody Dense Phases for Subcutaneous Delivery. Mol Pharm 2013.
3. Galush WJ, Le LN, Moore JM. Viscosity behavior of high-concentration protein mixtures. J Pharm Sci. 2012;101:1012–20.
4. Narasimhan C, Mach H, Shameem M. High-dose monoclonal antibodies via the subcutaneous route: challenges and technical solutions, an industry perspective. Ther Deliv. 2012;3:889–900.
5. Jezek J, Rides M, Derham B, Moore J, Cerasoli E, Simler R, *et al.* Viscosity of concentrated therapeutic protein compositions. Adv Drug Deliv Rev. 2011;63:1107–17.
6. Cromwell ME, Hilario E, Jacobson F. Protein aggregation and bioprocessing. AAPS J. 2006;8:E572–9.
7. Lilyestrom WG, Yadav S, Shire SJ, Scherer TM. Monoclonal antibody self-association, cluster formation, and rheology at high concentrations. J Phys Chem B. 2013;117:6373–84.
8. Guo Z, Chen A, Nassar RA, Helk B, Mueller C, Tang Y, *et al.* Structure-activity relationship for hydrophobic salts as viscosity-lowering excipients for concentrated solutions of monoclonal antibodies. Pharm Res. 2012;29:3102–9.
9. Kamerzell TJ, Pace AL, Li M, Danilenko DM, McDowell M, Gokarn YR, *et al.* Polar solvents decrease the viscosity of high concentration IgG1 solutions through hydrophobic solvation and interaction: formulation and biocompatibility considerations. J Pharm Sci. 2013;102:1182–93.
10. Srinivasan C, Weight AK, Bussemer T, Klibanov AM. Non-aqueous suspensions of antibodies are much less viscous than equally concentrated aqueous solutions. Pharm Res. 2013;30:1749–57.
11. He F, Becker GW, Litowski JR, Narhi LO, Brems DN, Razinkov VI. High-throughput dynamic light scattering method for measuring viscosity of concentrated protein solutions. Anal Biochem. 2010;399:141–3.
12. Connolly BD, Petry C, Yadav S, Demeule B, Ciaccio N, Moore JM, *et al.* Weak interactions govern the viscosity of concentrated antibody solutions: high-throughput analysis using the diffusion interaction parameter. Biophys J. 2012;103:69–78.
13. He F, Woods CE, Trilisky E, Bower KM, Litowski JR, Kerwin BA, Becker GW, Narhi LO, Razinkov VI. Screening of monoclonal antibody formulations based on high-throughput thermostability and viscosity measurements: Design of experiment and statistical analysis. J Pharm Sci 2010.
14. Agrawal NJ, Kumar S, Wang X, Helk B, Singh SK, Trout BL. Aggregation in protein-based biotherapeutics: computational studies and tools to identify aggregation-prone regions. J Pharm Sci. 2011;100:5081–95.
15. Chennamsetty N, Voynov V, Kayser V, Helk B, Trout BL. Design of therapeutic proteins with enhanced stability. Proc Natl Acad Sci U S A. 2009;106:11937–42.
16. Wang X, Das TK, Singh SK, Kumar S. Potential aggregation prone regions in biotherapeutics: a survey of commercial monoclonal antibodies. MAbs. 2009;1:254–67.
17. Wang X, Singh SK, Kumar S. Potential aggregation-prone regions in complementarity-determining regions of antibodies and their contribution towards antigen recognition: a computational analysis. Pharm Res. 2010;27:1512–29.
18. Wang X, Kumar S, Buck PM, Singh SK. Impact of deglycosylation and thermal stress on conformational stability of a full length murine IgG2a monoclonal antibody: Observations from molecular dynamics simulations. Proteins. 2013;81:443–60.
19. Buck PM, Kumar S, Wang X, Agrawal NJ, Trout BL, Singh SK. Computational methods to predict therapeutic protein aggregation. Methods Mol Biol. 2012;899:425–51.
20. Buck PM, Kumar S, Singh SK. Insights into the potential aggregation liabilities of the b12 Fab fragment via elevated temperature molecular dynamics. Protein Eng Des Sel. 2013;26:195–206.
21. Buck PM, Kumar S, Singh SK On the role of aggregation prone regions in protein evolution, stability, and enzymatic catalysis: insights from diverse analyses. PLoS Comp Biol. In press: 2013.
22. Yadav S, Laue TM, Kalonia DS, Singh SN, Shire SJ. The influence of charge distribution on self-association and viscosity behavior of monoclonal antibody solutions. Mol Pharm. 2012;9:791–802.
23. Yadav S, Sreedhara A, Kanai S, Liu J, Lien S, Lowman H, *et al.* Establishing a link between amino acid sequences and self-associating and viscoelastic behavior of two closely related monoclonal antibodies. Pharm Res. 2011;28:1750–64.
24. Harn N, Allan C, Oliver C, Middaugh CR. Highly concentrated monoclonal antibody solutions: direct analysis of physical structure and thermal stability. J Pharm Sci. 2007;96:532–46.
25. Kamerzell TJ, Kanai S, Liu J, Shire SJ, Wang YJ. Increasing IgG concentration modulates the conformational heterogeneity and bonding network that influence solution properties. J Phys Chem B. 2009;113:6109–18.
26. Neergaard MS, Kalonia DS, Parshad H, Nielsen AD, Moller EH, van de Weert M. Viscosity of high concentration protein formulations of monoclonal antibodies of the IgG1 and IgG4 subclass - prediction of viscosity through protein-protein interaction measurements. Eur J Pharm Sci. 2013;49:400–10.
27. Chaudhri A, Zarraga IE, Kamerzell TJ, Brandt JP, Patapoff TW, Shire SJ, *et al.* Coarse-grained modeling of the self-association of therapeutic monoclonal antibodies. J Phys Chem B. 2012;116:8045–57.
28. Chaudhri A, Zarraga IE, Yadav S, Patapoff TW, Shire SJ, Voth GA. The role of amino acid sequence in the self-association of therapeutic monoclonal antibodies: insights from coarse-grained modeling. J Phys Chem B. 2013;117:1269–79.
29. Yadav S, Shire SJ, Kalonia DS. Viscosity behavior of high-concentration monoclonal antibody solutions: correlation with interaction parameter and electroviscous effects. J Pharm Sci. 2012;101:998–1011.
30. Laue T. Proximity energies: a framework for understanding concentrated solutions. J Mol Recognit. 2012;25:165–73.
31. Yadav S, Shire SJ, Kalonia DS. Factors affecting the viscosity in high concentration solutions of different monoclonal antibodies. J Pharm Sci. 2010;99:4812–29.
32. Yadav S, Liu J, Shire SJ, Kalonia DS. Specific interactions in high concentration antibody solutions resulting in high viscosity. J Pharm Sci. 2010;99:1152–68.
33. Saito S, Hasegawa J, Kobayashi N, Kishi N, Uchiyama S, Fukui K. Behavior of monoclonal antibodies: relation between the second virial coefficient (B (2)) at low concentrations and aggregation propensity and viscosity at high concentrations. Pharm Res. 2012;29:397–410.
34. Warne NW. Development of high concentration protein biopharmaceuticals: the use of platform approaches in formulation development. Eur J Pharm Biopharm. 2011;78:208–12.
35. Bolton GR, Boesch AW, Basha J, Lacasse DP, Kelley BD, Acharya H. Effect of protein and solution properties on the Donnan effect during the ultrafiltration of proteins. Biotechnol Prog. 2011;27:140–52.
36. Creighton TE The physical and chemical basis of molecular biology, Helvetian Press, 2010.
37. Saphire EO, Stanfield RL, Crispin MD, Morris G, Zwick MB, Pantophlet RA, *et al.* Crystal structure of an intact human IgG: antibody asymmetry, flexibility, and a guide for HIV-1 vaccine design. Adv Exp Med Biol. 2003;535:55–66.

38. Berman HM, Westbrook J, Feng Z, Gilliland G, Bhat TN, Weissig H, *et al.* The protein data bank. Nucleic Acids Res. 2000;28:235–42.
39. Fernandez-Escamilla AM, Rousseau F, Schymkowitz J, Serrano L. Prediction of sequence-dependent and mutational effects on the aggregation of peptides and proteins. Nat Biotechnol. 2004;22: 1302–6.
40. Maurer-Stroh S, Debulpaep M, Kuemmerer N, Lopez de la Paz M, Martins IC, Reumers J, *et al.* Exploring the sequence determinants of amyloid structure using position-specific scoring matrices. Nat Methods. 2010;7:237–42.
41. Mant CT, Kovacs JM, Kim HM, Pollock DD, Hodges RS. Intrinsic amino acid side-chain hydrophilicity/hydrophobicity coefficients determined by reversed-phase high-performance liquid chromatography of model peptides: comparison with other hydrophilicity/ hydrophobicity scales. Biopolymers. 2009;92:573–95.
42. Plimpton SJ. Fast parallel algorithms for short-range molecular dynamics. J Comp Physiol. 1995;117:1–19.
43. Medhi J. Statistical methods: An introductory text. New Delhi: Wiley Eastern Limited; 1992.
44. Minton AP. Influence of macromolecular crowding upon the stability and state of association of proteins: predictions and observations. J Pharm Sci. 2005;94:1668–75.
45. Mooney M. The viscosity of a concentrated suspension of spherical particles. J Colloid Sci. 1951;6:162–70.
46. Teplyakov A, Zhao Y, Malia TJ, Obmolova G, Gilliland GL. IgG2 Fc structure and the dynamic features of the IgG CH2-CH3 interface. Mol Immunol. 2013;56:131–9.
47. Davies AM, Rispens T, Ooijevaar-de Heer P, Gould HJ, Jefferis R, Aalberse RC, *et al.* Structural determinants of unique properties of human IgG4-Fc. J Mol Biol. 2014;426:630–44.
48. Ely KR, Herron JN, Harker M, Edmundson AB. Three-dimensional structure of a light chain dimer crystallized in water. Conformational flexibility of a molecule in two crystal forms. J Mol Biol. 1989;210: 601–15.
49. Vincentand KJ, Zurini M. Current strategies in antibody engineering: Fc engineering and pH-dependent antigen binding, bispecific antibodies and antibody drug conjugates. Biotechnol J. 2012;7:1444–50.
50. Vafa O, Gilliland GL, Brezski RJ, Strake B, Wilkinson T, Lacy ER, *et al.* An engineered Fc variant of an IgG eliminates all immune effector functions via structural perturbations. Methods. 2014;65: 114–26.
51. Saltzman WM, Radomsky ML, Whaley KJ, Cone RA. Antibody diffusion in human cervical mucus. Biophys J. 1994;66:508–15.
52. Miao L, Qin H, Koehl P, Song J. Selective and specific ion binding on proteins at physiologically-relevant concentrations. FEBS Lett. 2011;585:3126–32.
53. Gokarn YR, Fesinmeyer RM, Saluja A, Razinkov V, Chase SF, Laue TM, *et al.* Effective charge measurements reveal selective and preferential accumulation of anions, but not cations, at the protein surface in dilute salt solutions. Protein Sci. 2011;20:580–7.
54. Lehermayr C, Mahler HC, Mader K, Fischer S. Assessment of net charge and protein-protein interactions of different monoclonal antibodies. J Pharm Sci. 2011;100:2551–62.
55. Laue T. How solvent and excipient properties impact aggregation and viscosity. Palm Springs: CHI PepTalk; 2013.
56. Bas DC, Rogers DM, Jensen JH. Very fast prediction and rationalization of pKa values for protein-ligand complexes. Proteins. 2008;73:765–83.
57. Rostkowski M, Olsson MH, Sondergaard CR, Jensen JH. Graphical analysis of pH-dependent properties of proteins predicted using PROPKA. BMC Struct Biol. 2011;11:6.
58. Kieseritzkyand G, Knapp EW. Optimizing pKa computation in proteins with pH adapted conformations. Proteins. 2008;71:1335–48.